LASER & PHOTONICS REVIEWS

www.lpr-journal.org

Single Pulse Manipulations in Synthetic Time-Frequency Space

Guangzhen Li, Danying Yu, Luqi Yuan, and Xianfeng Chen*

Synthetic dimensions in photonic structures provide unique opportunities for actively manipulating light in multiple degrees of freedom. Here, a dispersive waveguide under the dynamic phase modulation is theoretically explored, which supports single pulse manipulations in the synthetic (2+1) dimensions. Compared with the counterpart of the conventional (2+1) space-time, temporal diffraction and frequency conversion in a synthetic time-frequency space are demonstrated while the pulse evolves along the spatial dimension. It is found that a rich set of pulse propagation behaviors can be achieved by introducing the effective non-uniform gauge potential for photons in the synthetic time-frequency space with the control of the modulation phase, including confined pulse propagation, fast/slow light, and pulse compression. With the additional nonperiodic oscillation subject to the effective force along the frequency axis of light, this work provides an exotic approach for actively manipulating the single pulse in both temporal and spectral domains, which shows the great promise for applications of the pulse processing and optical communications in integrated photonics.

1. Introduction

Synthetic dimension in photonics is an emergent field for exploring physics in higher-dimensional space within lower-geometrical structure, which also points toward manipulating light by utilizing physical phenomena in the synthetic space.[1,2] Different degrees of freedom of photons can be used to construct synthetic dimensions, such as frequencies,[3–6] orbital angular momenta,[7] pulse arrival times,[8,9] and others.[10–12] With synthetic dimensions, many potential applications have been proposed, including unidirectional frequency translation,[13] orbital angular momentum switch,[14] pulse narrowing,[15] and mode-locked topological laser.[16] Furthermore, it has also been shown that one can simultaneously build up two synthetic dimensions with different degrees of freedom of light and explore topological edge states.[17,18] This synthetic (2+1) dimensions require only one single cavity, which dramatically simplify the experimental requirements.

Group velocity dispersion (GVD) is a fundamental optical characteristic in a medium, and is of great importance in ultrashort pulse manipulations,[19–21] such as pulse compression,[22–24] generation of optical solitons,[25,26] and group velocity control,[27–29] where the interplay between dispersive and nonlinear effects on optical pulses takes place.[30] Moreover, it has been found that, when a pulse propagates along a dispersive waveguide, one can consider the problem in a synthetic (1+1) dimensions, that is, the optical field diffracts along a time dimension when it evolves along the spatial dimension.[31–33]

In this work, we move a step further and show the possibility of multiple single pulse manipulations in synthetic (2+1) dimensions including the temporal diffraction and frequency conversion in a synthetic time-frequency space while a pulse propagates along the spatial dimension. A dispersive waveguide incorporating segmented electrodes under travelling wave electro-optic modulation is considered (see **Figure 1**a). We show that one constructs a 2D synthetic space including the time and frequency dimensions, and pulse dynamics is studied when the spatial propagating dimension is treated as the synthetic time evolution. An effective gauge potential core is constructed in synthetic two dimensions with non-uniform distribution of modulation phases to confine light.[34–36] By manipulating the effective gauge potential core in multiple ways, we show rich physics of pulse manipulations, including confined pulse propagation, fast/slow light, and pulse compression. Fundamentally different from previous works,[31–33] our results link to physics in (2+1) dimensions, which points out exotic route toward manipulating pulse profile and frequency conversion process. Our work can find important applications of optical pulse engineering in various platforms, ranging from second/third-order dispersive waveguide-based systems to on-chip dispersive microresonator-based systems.

G. Li, D. Yu, L. Yuan, X. Chen
State Key Laboratory of Advanced Optical Communication Systems and Networks
School of Physics and Astronomy
Shanghai Jiao Tong University
Shanghai 200240, China
E-mail: yuanluqi@sjtu.edu.cn
X. Chen
Shanghai Research Center for Quantum Sciences
Shanghai 201315, China
X. Chen
Jinan Institute of Quantum Technology
Jinan 250101, China
X. Chen
Collaborative Innovation Center of Light Manipulation and Applications
Shandong Normal University
Jinan 250358, China

The ORCID identification number(s) for the author(s) of this article can be found under https://doi.org/10.1002/lpor.202100340

DOI: 10.1002/lpor.202100340

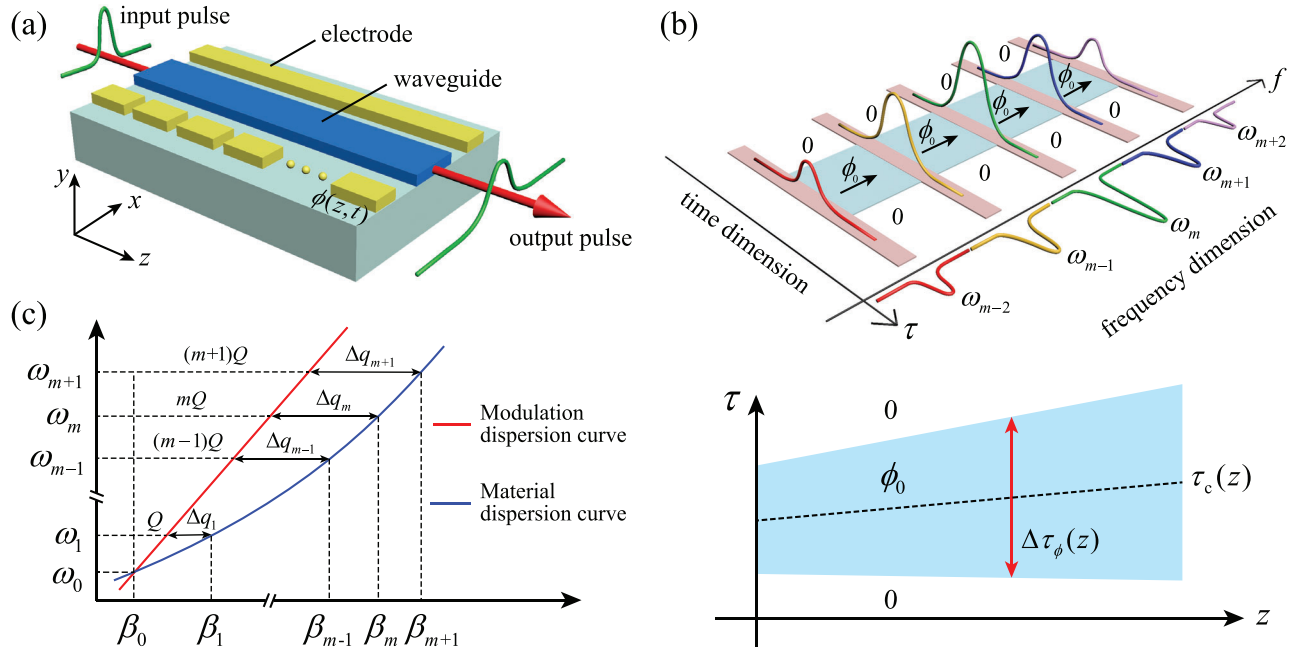

Figure 1. a) A pulse propagating through a waveguide with segmented electrodes for modulations. b) The system in (a) can be mapped into a synthetic (2+1) dimensions, where an effective gauge potential is constructed in the time-frequency space by non-uniform phase modulation (the upper panel). The lower panel: A schematic of a time-dependent and spatially non-uniform modulation phase $\phi(z, \tau)$ described in Equation (2), where the non-zero phase ϕ_0 denotes an effective gauge potential core with the labeled width $\Delta\tau_\phi(z)$ (red arrow) and center $\tau_c(z)$ (dashed line) along the temporal dimension τ at each z. c) Dispersion curves for waveguide (blue line) and modulation (red line).

2. Theoretical Model of the Synthetic Time-frequency Space

2.1. Physical Concept

We begin with briefly illustrating synthetic (2+1) dimensions constructed in a waveguide shown in Figure 1a, modulated by a traveling wave with a sinusoidal radio frequency (RF) signal. The refractive index is governed by[37]

$$n(z,t) = n_0 + \Delta n \cos[\Omega t - Qz + \phi(z,t)] \tag{1}$$

where n_0 is static refractive index and Δn is the modulation amplitude. Ω, Q, and ϕ are the frequency, wavevector, and modulation phase of the RF signal. For a pulse centered at the frequency ω_0 propagating along the spatial dimension z, the applied modulation connects field components at discrete frequencies $\omega_m = \omega_0 + m\Omega$, and forms the synthetic frequency dimension (see Figure 1b).[6] On the other hand, for a dispersive waveguide, the pulse experiences temporal diffraction, which brings up the concept of the synthetic dimension along the continuous retarded time frame ($\tau = t - z/v_g$, with v_g being the group velocity at ω_0).[30,31] Hence, a synthetic continuous-discrete time-frequency space is constructed for the pulse travelling along z-direction inside the waveguide.

It has been demonstrated by Lin et al. that different gauge potentials in a discrete resonator lattice under dynamic modulations can guide light spatially.[34] Here, we extend this mechanism to the proposed synthetic continuous-discrete time-frequency space by considering a time-dependent and spatially non-uniform modulation phase $\phi(z, \tau)$:

$$\phi(z,\tau) = \begin{cases} \phi_0 & |\tau - \tau_c(z)| \le \Delta\tau_\phi(z) \\ 0 & |\tau - \tau_c(z)| > \Delta\tau_\phi(z) \end{cases} \tag{2}$$

that is, at any z, the hopping phase along the frequency dimension is ϕ_0 in a core region with the center $\tau_c(z)$ and width $\Delta\tau_\phi(z)$, and equals to 0 at the remaining regions (see Figure 1b). Such phase distribution can be achieved by controlling RF signals at each segmented electrode and supports the effective gauge potential distribution in the synthetic space.[38] The sharp interface of the square-shape phase distribution in Equation (2) brings higher effective gauge potential difference, and can better confine light in the core region,[39,40] where the largest difference occurs at $\phi_0 = \pi$.[34] We label the middle temporal-spatial region flexibly formed by non-zero phase ϕ_0 as an effective gauge potential core (see Figure 1b), which can be used to manipulate single pulse in different ways. Different from the conventional or temporal waveguide that guides light by constructing spatial or temporal refractive index interface,[33,41] the time-averaging refractive index profile is uniform in our system.

2.2. Theoretical Analysis

We now build detailed theoretical framework to study the system. The waveguide in Figure 1a can support a finite number of guided modes, where only the fundamental guided mode is considered in our model for simplicity. The electric vector of the

fundamental guided mode can be written as $\mathbf{E}(\mathbf{r},t)=\mathscr{E}(r_\perp)E(z,t)$ by using the method of separation of variables with $\mathscr{E}(r_\perp)$ being the modal profile of the waveguide.[30,42] For pulse propagating through the modulated waveguide, the electric field of the pulse can be expanded as $E(z,t)=\sum_m a_m(z,t)e^{i(\omega_m t-\beta_m z)}$, where all components labeled by m correspond to the fundamental guided mode of the waveguide.[30,42] Here, $a_m(z,t)$ is the slowly-varying envelope for the frequency component at ω_m.[3,6] The propagation constant β_m is not equally spaced due to GVD (see Figure 1c), which can be defined as $\beta_m=\beta_0+mQ+\Delta q_m$. Here, β_0 is the wavevector associated with ω_0, and Δq_m denotes the wavevector mismatching. The pulse field follows the wave equation (see Supporting Information)

$$\frac{\partial^2 E(z,t)}{\partial z^2}-\frac{1}{\epsilon_0 c^2}\frac{\partial^2[\epsilon_0\epsilon_r(z,t)E(z,t)]}{\partial t^2}=0 \tag{3}$$

where ϵ_0 and $\epsilon_r(z,t)=n^2(z,t)$ are vacuum and relative permittivity, respectively. With the expansion of the field, we obtain the propagating equations for m^{th} component in the retarded frame

$$i\frac{\partial a_m(z,\tau)}{\partial z}=-\frac{k_2}{2}\frac{\partial^2 a_m}{\partial\tau^2}+g[a_{m+1}e^{-i(c_1+c_2+2c_2m)z-i\phi(z,\tau)}+a_{m-1}e^{i(c_1-c_2+2c_2m)z+i\phi(z,\tau)}] \tag{4}$$

Here, $c_1=k_1\Omega-Q$ is linear mismatching between light and RF signal, and $c_2=k_2\Omega^2/2$ is quadratic mismatching caused by GVD, where k_1 and k_2 are Taylor expansion coefficients of wavevector $k(\omega)$ around ω_m, representing the reciprocal of the group velocity and GVD, respectively. $g=\Delta n\omega_0/2c$ denotes the coupling strength,

Equation (4) describes the dynamics of a pulse with multiple frequency components at ω_m propagating along z-axis in a reference frame moving at v_g. The first term on right-band side of Equation (4) dominates the pulse dispersion behavior, which is a counterpart of wave diffusion in the spatial dimension, while the second term refers to frequency conversions. Equation (4) has the form of the Schrödinger equation within (2+1) dimensions,[30,43] where the pulse experiences continuous temporal diffraction and discrete frequency conversion in two synthetic dimensions while it evolves at z-axis (see Figure 1b). Moreover, the hopping phase in Equation (4) gives an effective non-uniform force $F=c_1+2c_2m+\partial\phi/\partial z$ pointing along the frequency dimension.[13] Different from previous studies, which have explored consequences of an effective uniform force in the synthetic frequency dimension,[6,13,44] here the effective force varies with z due to GVD. Yet, as we show in the following, a synthetic time-frequency space together with the non-uniform force give us alternative opportunity for manipulating the pulse propagation in the waveguide.

3. Simulation Results of Single Pulse Manipulations

We simulate pulse propagations by Equation (4) with excitations at one end of the waveguide at $z=0$. The input pulse has a profile as $f(\tau)=e^{-1.386[\tau/\Delta\tau]^2}$, where $\Delta\tau=30$ ps is the temporal full width at half maximum (FWHM). We assume that the input field contains only one frequency component at $\omega_0=1.2\times10^{15}$ Hz (or 1550 nm). Note that Equation (4) is valid when the condition $\Omega>\Delta\omega(z)$ is satisfied, that is, field profiles at different frequency components in the spectral domain do not overlap, where $\Delta\omega(z)$ is the spectral FWHM for each frequency component at any z. For the input pulse, $\Delta\omega=2\pi\cdot14.7$ GHz. The simulation is performed with 21 modes ($m=-10,\dots,10$). **Figure 2**a shows the profile of the input pulse in the synthetic time-frequency space.

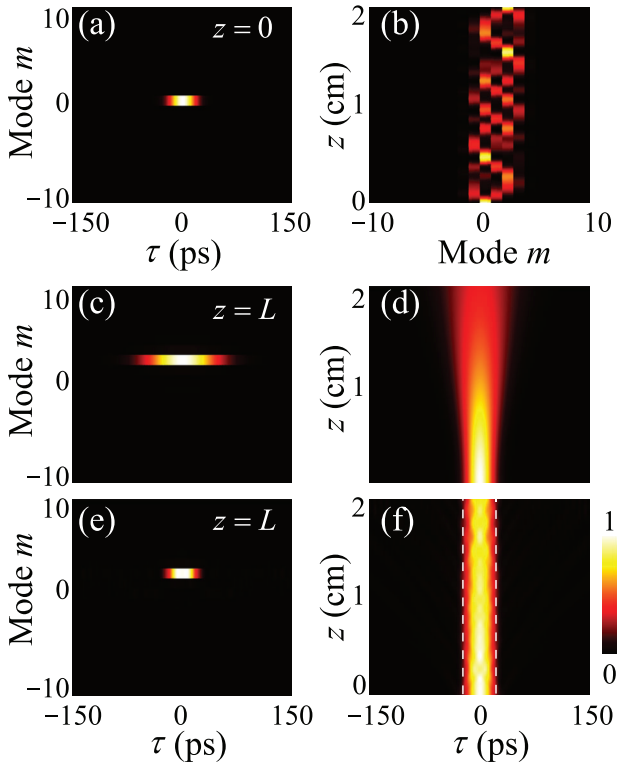

Figure 2. Pulse propagations under b–d) constant modulation and e,f) modulation with effective gauge potential core labeled by dashed line. a,c,e) Intensity distribution $|a_m(z,\tau)|^2$ at $z=0$ and $z=L$ in the synthetic time-frequency space. b) Evolution of intensities for each mode $I_m(z)\equiv\int_\tau|a_m(z,\tau)|^2\mathrm{d}\tau$. d,f) evolution of the pulse $I(z,\tau)\equiv\sum_m|a_m(z,\tau)|^2$.

First, we consider the normal case that pulse propagates in the waveguide under the modulation with $\phi(z,\tau)=0$. We choose modulation with $\Delta n=5\times10^{-4}$ and $\Omega=2\pi\cdot29.4$ GHz, which gives $g=10^3$ m^{-1}. For the waveguide with a length $L=2$ cm, we have $k_2=4\times10^{-20}$ m^{-1}s^2, which leads to $c_2=682$ m^{-1}. c_1 can be approximated to be zero by tuning $Q=k_1\Omega$. All parameters are chosen with the experimental feasibility in the literature.[45–47]

When the pulse evolves along the z-axis, it experiences frequency conversion and nonperiodic oscillation near the 0th mode in the frequency dimension under the effective non-uniform force (see Figure 2b). At $L=2$ cm, frequency components of pulse oscillate back to the single mode, which shifts to the 2nd mode (see Figure 2c). Note that the conventional Bloch oscillation is periodic under an effective uniform force.[13] Moreover, the pulse gets broadened due to GVD and has the temporal width $\Delta\tau(z=L)=79$ ps, as shown in Figure 2c,d. It agrees well with the

theoretical calculated evolution of the pulse width for a Gaussian pulse (see Figure S1a, Supporting Information).

3.1. Confined Pulse Propagation

We next consider modulations with non-uniform distributions of phases and explore the dynamics from Equation (4) under effective non-uniform gauge potential. We choose parameters $\phi_0 = \pi$, $\tau_c(z) = 0$ and $\Delta\tau_\phi(z) = 30$ ps, which indicate a fixed effective gauge potential core in the synthetic space. The simulation shows the confinement of light in the middle region of the effective gauge potential core (labeled by the dashed line) in the synthetic time dimension as shown in Figure 2e,f, while the frequency component is shifted to the 2nd mode as the previous case. The pulse width remains 30 ps while maintaining an approximate Gaussian waveform during the propagation (see Figure S1b, Supporting Information). The result here shows an interesting combination between nonperiodic oscillation along the frequency dimension and the light confinement due to the effective non-uniform gauge potential in the time dimension. As a comparison, we calculate the evolution of pulse with $c_2 = 0$, with other parameters unchanged, and find temporal confinement of light persists while the frequency conversion covers a broad range of modes (see Figure S2, Supporting Information). Moreover, one can control the distribution of frequency components in the output pulse by using an input pulse with a Gaussian distribution of multiple modes. Unidirectional and bidirectional frequency transports together with temporal pulse manipulations can be achieved (see Figure S3, Supporting Information). Not only the confined pulse propagation demonstrated here, the idea of utilizing effective gauge potentials in synthetic time-frequency dimensions provides more different ways to manipulate the pulse.

3.2. Fast and Slow Light

We further shift the center of the effective gauge potential core linearly dependent on z with $\tau_c(z) = \eta_1 z$, where η_1 is the shift parameter. This choice makes the modulation phase taking the form of $\phi(z,\tau) = \pi$ for $|\tau - \eta_1 z| \le 30$ ps and zero for other τ. It provides a way to manipulate the group velocity of pulse controlled by η_1. In simulations, we use $\Omega = 2\pi \times 29.4$ GHz, $\Delta n = 10^{-3}$, and $k_2 = 6 \times 10^{-20}$ m^{-1}s^2, which give $g = 2 \times 10^3$ m^{-1}, and $c_2 = 1023$ m^{-1}. With a positive $\eta_1 = 22$ ps cm^{-1}, we find slow light with group velocity delay of 57 ps and pulse width of 27 ps as shown in **Figure 3**a,c. On the other hand, one can see the generation of fast light in Figure 3b,d with negative $\eta_1 = -22$ ps cm^{-1}. Here, large dispersion and strong modulation are chosen to efficiently manipulate the group velocity of the pulse. Figure 3e exhibits the output pulse profiles of slow and fast light at $z = L$, where the peak intensity decreases due to the dispersion loss. The corresponding nonperiodic oscillation for the slow light is plotted in Figure 3f, while the nonperiodic oscillation for the fast light is similar. At $z = L$, the output pulse has two major frequency components at 0th and 2nd modes (see Figure 3a,b). The single frequency conversion can be established by choosing a different propagation length. For example, one sees that oscillations shift to a single mode at $m = 2$ at $z = 1.63$ cm. Further larger group

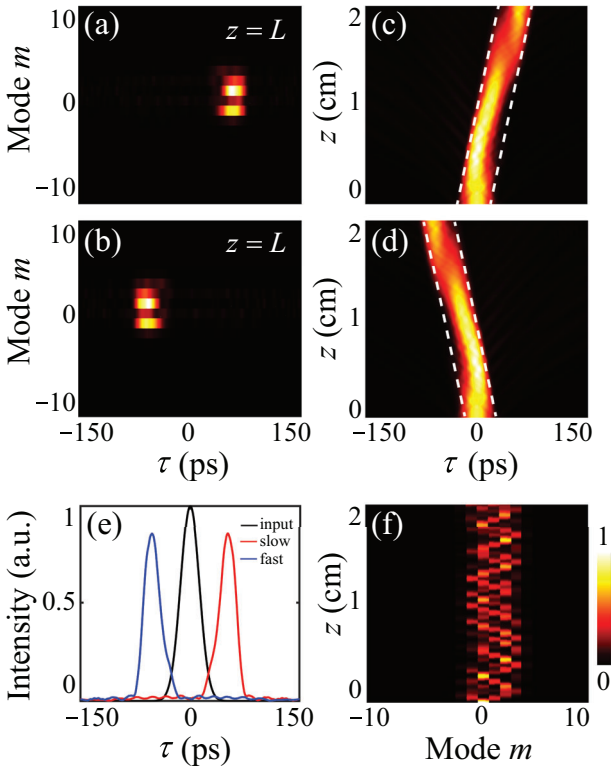

Figure 3. a,b) Intensity distribution $|a_m(z,\tau)|^2$ at $z = L$ in the synthetic time-frequency space. c,d) Evolution of the pulse $I(z,\tau)$. The effective gauge potential cores are labeled by dashed lines. e) The intensity profile of output pulse $I(z = L,\tau)$ in (a) (red line) and (b) (blue line), compared with input pulse $I(z = 0,\tau)$ (black line). f) Evolution of intensities for each mode $I_m(z)$ with effective potential core in (c).

velocity manipulation can be obtained by using larger $|\eta_1|$ and GVD at the cost of the intensity loss. We note that, in these fast and slow light manipulations, an input pulse centered at ω_0 can be converted to multiple temporally overlapped pulses centered at discrete frequencies ω_m, where each one at ω_m has its pulse profile nearly unchanged compared with the input one.

3.3. Pulse Compression

The width of effective gauge potential core can also be used to control the pulse width. We consider a varying gauge potential core along z with $\Delta\tau_\phi(z) = 30 - \eta_2 z$ and $\tau_c(z) = 0$, where η_2 is the width-varying parameter. Thus, the configuration of modulation phase becomes $\phi(z,\tau) = \pi$ for $|\tau| \le 30 - \eta_2 z$ ps and zero for other τ. We take parameters $\eta_2 = 12.5$ ps cm^{-1}, $k_2 = 6 \times 10^{-21}$ m^{-1}s^2, $\Delta n = 10^{-3}$, and $\Omega = 2\pi \times 88.2$ GHz, which lead to $g = 2 \times 10^3$ m^{-1} and $c_2 = 920$ m^{-1} in the simulation and show results in **Figure 4**. Figure 4a shows the pulse profile in the synthetic time-frequency space at $z = L$. Although the pulse converts to multiple modes, the temporal width of the pulse is largely compressed. As shown in Figure 4b, the narrowing of the effective gauge potential core forces pulse compression gradually while it propagates along the z-axis. Figure 4c plots the pulse width versus z, showing a trend of overall decrease. The output pulse profile has width of 5 ps, with the enhanced

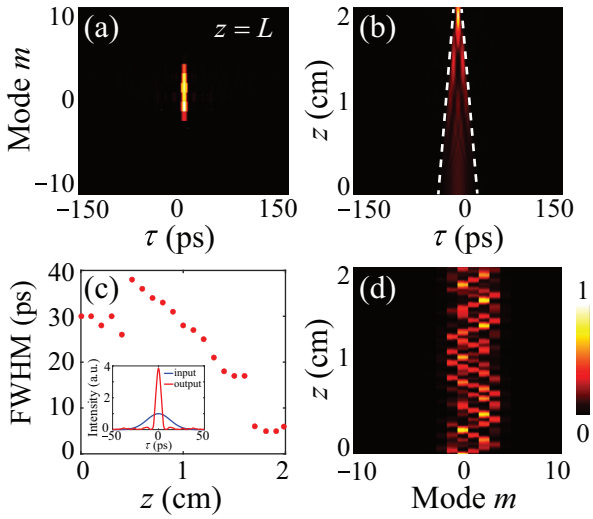

Figure 4. a) Intensity distribution $|a_m(z,\tau)|^2$ at $z = L$ in the synthetic time-frequency space. b) Evolution of the pulse $I(z,\tau)$, where the effective gauge potential cores are labeled by dashed lines. c) Evolution of the pulse width $\Delta\tau(z)$ calculated from (b). Inserted: the intensity profile of output pulse $I(z = L,\tau)$ in (a) (red line) compared with input pulse $I(z = 0,\tau)$ (blue line). d) Evolution of intensities for each mode $I_m(z)$.

peak intensity. Simultaneously, the frequency conversion follows nonperiodic oscillation as shown in Figure 4d. The output with multiple frequency components can be tuned by changing the length of the waveguide. For example, at $z = 1.64$ cm, the field exhibits one major frequency component at the 2nd mode. As the last note, the pulse compression cannot lead to an output field with an infinitely small temporal width (broad frequency bandwidth). The condition $\Omega > \Delta\omega(z)$ at any z shall be satisfied.

4. Discussion and Conclusion

We propose a modulated waveguide system with parameters based on lithium–niobate waveguide system. The numbers used in simulations require waveguide with large dispersion and fast electro-optic modulation, which are experimentally achievable in the second-order nonlinear waveguide with the state-of-art technology. Dispersion near 10^{-22} $m^{-1}s^2$ has been reported,[46] which can be further enlarged by structure engineering or operating at higher dispersion wavelength. $\Delta n = 10^{-3}$ corresponds to 7 V μm^{-1} voltage amplitude of an applied external electric field. If larger modulation is needed, high voltage up to 65 V μm^{-1} has been demonstrated.[45] Note that the modulation amplitude Δn should be large enough to compensate the pulse dispersion (labeled by k_2) for achieving effective light confinement. Larger modulation amplitude results in faster frequency conversion efficiency, which shall not hinder pulse manipulations. The modulation amplitudes we choose in the simulations are around the minimum required values. Shorter pulse manipulation is possible with smaller dispersion but larger modulation frequency, such as 100 GHz, which is commercially available.[47] The choice of ω_0 in our simulations can be arbitrary as long as the generated frequency modes are still in the vicinity of the fundamental guided mode of the waveguide. Moreover, recent advances of integrated waveguide platform bring opportunity to achieve synthetic time-frequency dimensions in integrated photonics, on which modulators with frequency ≈200 GHz have been demonstrated.[48] The construction of a synthetic time-frequency space can be further extended beyond by adding other degrees of freedom such as orbital angular momentum or pseudospin.[7,18] Besides, our analysis shall be valid for other systems if one scales parameters consistently. The modulation phase in the core region is chosen as $\phi_0 = \pi$ for generating the largest effective gauge potential contrast to efficiently confine light, while other values of phases might lead to potential applications in one-way frequency conversion in the synthetic space.[34] Our model shows promise for studying pulse propagating in dispersive resonators with synthetic dimensions,[49] and in third-order dispersive waveguide or microresonator-based systems.[50–53]

In summary, we propose synthetic (2+1) dimensions for manipulating pulse propagation in a dispersive waveguide under dynamic modulations. With the effective non-uniform gauge potential for photons and nonperiodic oscillation in the synthetic space, multiple pulse propagation behaviors including confined pulse propagation, fast/slow light, and pulse compression have been shown. Our work provides an alternative platform for actively manipulating single pulse in different ways, which is highly re-configurable, and hence shows promising potentials for pulse engineering in integrated photonics and optical communications.[54]

Supporting Information

Supporting Information is available from the Wiley Online Library or from the author.

Acknowledgements

The research was supported by the National Natural Science Foundation of China (11974245), the National Key R&D Program of China (2017YFA0303701), the Shanghai Municipal Science and Technology Major Project (2019SHZDZX01), the Natural Science Foundation of Shanghai (19ZR1475700), and the China Postdoctoral Science Foundation (2020M671090). L.Y. acknowledges support from the Program for Professor of Special Appointment (Eastern Scholar) at Shanghai Institutions of Higher Learning. X.C. also acknowledges the support from Shandong Quancheng Scholarship (00242019024).

Conflict of Interest

The authors declare no conflict of interest.

Data Availability Statement

The data that support the findings of this study are available from the corresponding author upon reasonable request.

Keywords

dynamic phase modulation, non-uniform gauge potential, pulse manipulation, synthetic time-frequency dimensions

Received: June 23, 2021
Revised: September 17, 2021
Published online:

[1] L. Yuan, Q. Lin, M. Xiao, S. Fan, *Optica* **2018**, *5*, 1396.
[2] T. Ozawa, H. M. Price, *Nat. Rev. Phys.* **2019**, *1*, 349.
[3] L. Yuan, Y. Shi, S. Fan, *Opt. Lett.* **2016**, *41*, 741.
[4] T. Ozawa, H. M. Price, N. Goldman, O. Zilberberg, I. Carusotto, *Phys. Rev. A* **2016**, *93*, 043827.
[5] B. A. Bell, K. Wang, A. S. Solntsev, D. N. Neshev, A. A. Sukhorukov, B. J. Eggleton, *Optica* **2017**, *4*, 1433.
[6] C. Qin, F. Zhou, Y. Peng, D. Sounas, X. Zhu, B. Wang, J. Dong, X. Zhang, A. Alù, P. Lu, *Phys. Rev. Lett.* **2018**, *120*, 133901.
[7] X. Luo, X. Zhou, C. Li, J. Xu, G. Guo, Z. Zhou, *Nat. Commun.* **2015**, *6*, 7704.
[8] A. Regensburger, C. Bersch, B. Hinrichs, G. Onishchukov, A. Schreiber, C. Silberhorn, U. Peschel, *Phys. Rev. Lett.* **2011**, *107*, 233902.
[9] A. Regensburger, C. Bersch, M.-A. Miri, G. Onishchukov, D. N. Christodoulides, U. Peschel, *Nature* **2012**, *488*, 167.
[10] E. Lustig, S. Weimann, Y. Plotnik, Y. Lumer, M. A. Bandres, A. Szameit, M. Segev, *Nature* **2019**, *567*, 356.
[11] L. J. Maczewsky, K. Wang, A. A. Dovgiy, A. E. Miroshnichenko, A. Moroz, M. Ehrhardt, M. Heinrich, D. N. Christodoulides, A. Szameit, A. A. Sukhorukov, *Nat. Photonics* **2020**, *14*, 76.
[12] K. Wang, B. A. Bell, A. S. Solntsev, D. N. Neshev, B. J. Eggleton, A. A. Sukhorukov, *Light Sci. Appl.* **2020**, *9*, 132.
[13] L. Yuan, S. Fan, *Optica* **2016**, *3*, 1014.
[14] X. W. Luo, C. Zhang, G. C. Guo, Z. W. Zhou, *Phys. Rev. A* **2018**, *97*, 043841.
[15] L. Yuan, Q. Lin, M. Xiao, A. Dutt, S. Fan, *APL Photonics* **2018**, *3*, 086103.
[16] Z. Yang, E. Lustig, G. Harari, Y. Plotnik, Y. Lumer, M. A. Bandres, M. Segev, *Phys. Rev. X* **2020**, *10*, 011059.
[17] L. Yuan, Q. Lin, A. Zhang, M. Xiao, X. Chen, S. Fan, *Phys. Rev. Lett.* **2019**, *122*, 083903.
[18] A. Dutt, Q. Lin, L. Yuan, M. Minkov, M. Xiao, S. Fan, *Science* **2020**, *367*, 59.
[19] W. H. Reeves, D. V. Skryabin, F. Biancalana, J. C. Knight, P. S. J. Russell, F. G. Omenetto, A. Efimov, A. J. Taylor, *Nature* **2003**, *424*, 511.
[20] S. W. Huang, H. Zhou, J. Yang, J. F. McMillan, A. Matsko, M. Yu, D. L. Kwong, L. Maleki, C. W. Wong, *Phys. Rev. Lett.* **2015**, *114*, 053901.
[21] S. Divitt, W. Zhu, C. Zhang, H. J. Lezec, A. Agrawal, *Science* **2019**, *364*, 890.
[22] N. G. R. Broderick, D. Taverner, D. J. Richardson, M. Ibsen, R. I. Laming, *Phys. Rev. Lett.* **1997**, *79*, 4566.
[23] P. Colman, C. Husko, S. Combrié, I. Sagnes, C. W. Wong, A. De Rossi, *Nat. Photonics* **2010**, *4*, 862.
[24] D. T. H. Tan, P. C. Sun, Y. Fainman, *Nat. Commun.* **2010**, *1*, 116.
[25] M. Stratmann, T. Pagel, F. Mitschke, *Phys. Rev. Lett.* **2005**, *95*, 143902.
[26] S. H. Lee, D. Y. Oh, Q. F. Yang, B. Shen, H. Wang, K. Y. Yang, Y. H. Lai, X. Yi, X. Li, K. Vahala, *Nat. Commun.* **2017**, *8*, 1295.
[27] G. M. Gehring, A. Schweinsberg, C. Barsi, N. Kostinski, R. W. Boyd, *Science* **2006**, *312*, 895.
[28] G. Li, Y. Chen, H. Jiang, Y. Liu, X. Liu, X. Chen, *Opt. Express* **2015**, *23*, 18345.
[29] T. Qin, J. Yang, F. Zhang, Y. Chen, D. Shen, W. Liu, L. Chen, X. Jiang, X. Chen, W. Wan, *Commun. Phys.* **2020**, *3*, 118.
[30] G. P. Agrawal, *Nonlinear Fiber Optics*, Elsevier Science, Amsterdam **2010**.
[31] U. Peschel, C. Bersch, G. Onishchukov, *Centr. Eur. J. Phys.* **2008**, *6*, 619.
[32] B. W. Plansinis, W. R. Donaldson, G. P. Agrawal, *Phys. Rev. Lett.* **2015**, *115*, 183901.
[33] B. W. Plansinis, W. R. Donaldson, G. P. Agrawal, *J. Opt. Soc. Am. B* **2016**, *33*, 1112.
[34] Q. Lin, S. Fan, *Phys. Rev. X* **2014**, *4*, 031031.
[35] Y. Lumer, M. A. Bandres, M. Heinrich, L. J. Maczewsky, H. Herzig-Sheinfux, A. Szameit, M. Segev, *Nat. Photonics* **2019**, *13*, 339.
[36] M. I. Cohen, C. Jörg, Y. Lumer, Y. Plotnik, E. H. Waller, J. Schulz, G. v. Freymann, M. Segev, *Light Sci. Appl.* **2020**, *9*, 200.
[37] F. Y. Gan, G. L. Yip, in *Applications of Photonic Technology 2*, Springer, New York **1997**, pp. 469–475.
[38] C. Qin, L. Yuan, B. Wang, S. Fan, P. Lu, *Phys. Rev. A* **2018**, *97*, 063838.
[39] I. Krasnokutska, J.-L. J. Tambasco, X. Li, A. Peruzzo, *Opt. Express* **2018**, *26*, 897.
[40] D. Zhu, L. Shao, M. Yu, R. Cheng, B. Desiatov, C. J. Xin, Y. Hu, J. Holzgrafe, S. Ghosh, A. Shams-Ansari, E. Puma, N. Sinclair, C. Reimer, M. Zhang, M. Lončar, *Adv. Opt. Photon.* **2021**, *13*, 242.
[41] M. A. Gaafar, T. Baba, M. Eich, A. Y. Petrov, *Nat. Photonics* **2019**, *13*, 737.
[42] A. Yariv, *Optical Electronics*, Saunders College Publishing, Philadelphia **1991**.
[43] L. Yuan, D. W. Wang, S. Fan, *Phys. Rev. A* **2017**, *95*, 033801.
[44] G. Li, Y. Zheng, A. Dutt, D. Yu, Q. Shan, S. Liu, L. Yuan, S. Fan, X. Chen, *Sci. Adv.* **2021**, *7*, eabe4335.
[45] M. Luennemann, U. Hartwig, G. Panotopoulos, K. Buse, *Appl. Phys. B* **2003**, *76*, 403.
[46] A. Kaushalram, S. A. Samad, G. Hegde, S. Talabattula, *IEEE Photon. J.* **2019**, *11*, 1.
[47] C. Wang, M. Zhang, X. Chen, M. Bertrand, A. Shams-Ansari, S. Chandrasekhar, P. Winzer, M. Lončar, *Nature* **2018**, *562*, 101.
[48] X. Liu, B. Xiong, C. Sun, Z. Hao, L. Wang, J. Wang, Y. Han, H. Li, J. Yu, Y. Luo in Conference on Lasers and Electro-Optics/Pacific Rim. Optical Society of America, 2020 C4C_3.
[49] Q. Shan, D. Yu, G. Li, L. Yuan, X. Chen, *Prog. Electromagn. Res.* **2020**, 169.
[50] I.-W. Hsieh, X. Chen, J. I. Dadap, N. C. Panoiu, R. M. Osgood, S. J. McNab, Y. A. Vlasov, *Opt. Express* **2006**, *14*, 12380.
[51] M. B. Mia, N. Jaidye, S. Kim, *Opt. Express* **2019**, *27*, 10426.
[52] X. Xue, Y. Xuan, Y. Liu, P.-H. Wang, S. Chen, J. Wang, D. E. Leaird, M. Qi, A. M. Weiner, *Nat. Photonics* **2015**, *9*, 594.
[53] K. Y. Yang, K. Beha, D. C. Cole, X. Yi, P. Del'Haye, H. Lee, J. Li, D. Y. Oh, S. A. Diddams, S. B. Papp, K. J. Vahala, *Nat. Photonics* **2016**, *10*, 316.
[54] Z. Chen, M. Segev, *eLight* **2021**, *1*, 2.